International Journal of Nanomedicine

Dovepress
open access to scientific and medical research

Open Access Full Text Article

ORIGINAL RESEARCH

Copperphosphotungstate Doped Polyanilines Nanorods for GSH-Depletion Enhanced Chemodynamic/NIR-II Photothermal Synergistic Therapy

Sheng Ye[1], Huichun Xiao[1], Jian Chen[1], Di Zhang[1], Li Qi[1], Ting Peng[2], Yanyang Gao[2], Qianbing Zhang[3], Jinqing Qu[2], Lei Wang[4], Ruiyuan Liu[1]

[1]Guangdong Provincial Key Laboratory of Medical Image Processing, School of Biomedical Engineering, Southern Medical University, Guangzhou, Guangdong, People's Republic of China; [2]School of Chemistry and Chemical Engineering, South China University of Technology, Guangzhou, Guangdong, People's Republic of China; [3]Cancer Research Institute, School of Basic Medical Sciences, Southern Medical University, Guangzhou, Guangdong, People's Republic of China; [4]College of Materials and Chemical Engineering, Key Laboratory of Inorganic Nonmetallic Crystalline and Energy Conversion Materials, China Three Gorges University, Yichang, People's Republic of China

Correspondence: Jinqing Qu; Ruiyuan Liu, Email cejqqu@scut.edu.cn; ruiyliu@smu.edu.cn

Introduction: The high concentration of glutathione (GSH) and hydrogen peroxide (H_2O_2) levels within the tumor microenvironment (TME) are the major obstacle to induce the unsatisfactory anticancer treatment efficiency. The synergistic cancer therapy strategies of the combination the GSH depletion enhanced chemodynamic therapy (CDT) with photothermal therapy (PTT) have been proved to be the promising method to significantly improve the therapeutic efficacy.

Methods: The copperphosphotungstate was incorporated into polyanilines to design copperphosphotungstate doped polyaniline nanorods (CuPW@PANI Nanorods) via chemical oxidant polymerization of aniline. The low long-term toxicity and biocompatibility were evaluated. Both in vitro and in vivo experiments were carried out to confirm the GSH depletion enhanced CDT/NIR-II PTT synergistic therapy.

Results: CuPW@PANI Nanorods feature biosafety and biocompatibility, strong NIR-II absorbance, and high photothermal-conversion efficiency (45.14%) in NIR-II bio-window, making them highly applicable for photoacoustic imaging and NIR-II PTT. Moreover, CuPW@PANI Nanorods could consume endogenous GSH to disrupt redox homeostasis and perform a Fenton-like reaction with H_2O_2 to produce cytotoxic •OH for the enhanced CDT. Furthermore, NIR-II photothermal-induced local hyperthermia accelerates •OH generation to enhance CDT, which realizes high therapeutic efficacy in vivo.

Conclusion: This study provides a proof of concept of GSH-depletion augmented chemodynamic/NIR-II photothermal therapy.

Keywords: copperphosphotungstate, NIR-II absorption nanorods, NIR-II photothermal therapy, GSH depletion, chemodynamic therapy, synergistic therapy

Introduction

Redox homeostasis, the balance between the generation and consumption of reactive oxygen species (ROS) in cells, is one of the most important intracellular physiological equilibriums for cell survival.[1–3] ROS, including hydroxyl radicals (•OH), superoxide anions ($•O_2^-$), and singlet oxygen ($^1O_2$), play an essential role in tumorigenesis, tumor progression, metastasis, and tumor therapy.[4–6] ROS modulate various cell signaling pathways, which are primarily mediated through the transcription factors NF-κB and STAT3, hypoxia-inducible factor-1α, kinases, growth factors, cytokines and other proteins, and enzymes; these pathways have been linked to inflammation, tumor survival, proliferation, invasion, angiogenesis, and metastasis of cancer.[7–9] Nowadays, efficiently breaking the redox homeostasis to boost ROS generation has become the promising strategy for the anticancer treatment. However, due to the abnormalities of tumor tissues, H_2O_2 was overproduced, which is one of the

Received: 1 December 2022
Accepted: 14 February 2023
Published: 12 March 2023

most important sources of ROS and promotes tumor growth and metastasis.[10,11] Moreover, a high concentration of glutathione (GSH, up to 10 mM) is observed in the tumor tissues, which is an important intracellular antioxidant to scavenge the cytotoxic ROS and keep the redox homeostasis.[12,13] As a result, boosting ROS generation or depletion of GSH is the main approach to break redox homeostasis. For promotion of ROS production, chemodynamic therapy (CDT) exploits Fenton or Fenton-like reaction to convert endogenous H_2O_2 into highly toxic •OH for the elimination of tumor cells.[14–16] For depletion of GSH, direct GSH oxidation,[17] enhancing GSH efflux,[18,19] and inhibiting GSH synthesis[20,21] are the main strategies to break the redox balance and enhance the therapeutic effect. Therefore, the design and preparation of novel CDT nanomaterials, which could improve intracellular ROS levels and reduce GSH concentration in tumor cells to break the redox homeostasis in tumor tissues, has emerged as optional for tumor-enhanced CDT.[22–26]

However, GSH depletion enhanced CDT is far from satisfactory due to their strict requirement of H_2O_2 level and overexpressed glutathione in tumor tissues. Therefore, exploitation of CDT enhancement strategy, such as laser-enhanced CDT performance, is still a challenge. For example, the increasing local temperature at the tumor site can improve the Fenton or Fenton-like reaction rate to augment the efficiency of CDT.[27,28] Up to now, considerable efforts have been devoted to develop multifunction nanomaterials for combined CDT/PTT, including Mo_2C-derived polyoxometalate,[29] Au@$Cu_{2-x}Se$ core-shell nanocrystals,[30] Cu_2MoS_4 nanocomposites,[31] Fe_3O_4@MIL-100 nanocomposite,[32] and Copper-olsalazine MOF.[33,34] Therefore, multimodal therapies based on •OH generation, GSH consumption, and photothermal therapy are imperative to maximize the tumor therapeutic effect.

Recently, the near-infrared II photothermal therapy (NIR-II PTT) based on NIR-II absorption nanomaterials has drawn much attention in tumor therapy, which exhibited low toxicity, precise spatiotemporal selectivity, small photo-nscattering, high specificity, and excellent maximum permissible exposure (MPE,1064 nm: 1 W/cm^2).[35–37] Previous investigation on NIR-II absorption nanomaterials dominantly focused on noble-metal nanoparticles,[38,39] transition metal chalcogenide,[40,41] nanocarbons,[42,43] rare-earth doped nanoparticles,[44,45] two-dimensional (2D) nanosheets,[46,47] phosphorus phthalocyanine,[48,49] and conducting polymer nanoparticles.[50,51] Polyanilines (PANI), as one of conducting polymers, have outstanding potential applications in biomedicine, such as antimicrobial therapy, drug delivery, bone regeneration, nerve regeneration, wound healing, and biosensor, because of their high electrical conductivity and biocompatibility caused by the hydrophilic nature, low-toxicity, good environmental stability, and nanostructured morphology.[52,53] Moreover, chemical-modified polyanilines exhibited strong NIR-II absorbance, desirable photothermal-conversion performance, and excellent photostability, which make them good candidates for applications in NIR-II photothermal therapy of tumor.[54–57] PANI surely represent a promising, but not yet completely explored, area of NIR-II photothermal therapy of tumor which calls for opportunities of deeper studies and developed research.

Copperphosphotungstate (CuPW), an essential member of polyoxotungstates, has been explored as an excellent catalyst to degrade organic pollutants.[58,59] Moreover, CuPW demonstrated the oxidation property for ROS generation and GSH depletion.[60] However, the insufficient therapeutic efficiency of CuPW makes its clinical use impractical. Addressing the challenges, in this work, we rationally incorporated the copperphosphotungstate into polyanilines to design copperphosphotungstate doped polyaniline nanorods (CuPW@PANI Nanorods) via chemical oxidant polymerization of aniline. CuPW@PANI Nanorods demonstrate low long-term toxicity and satisfactory biocompatibility. Moreover, CuPW@PANI Nanorods achieve effective NIR-II absorption to thermal ablation cells. Furthermore, by the virtue of Cu^{2+} ions, these nanorods exhibit the ability to deplete intracellular GSH and convert H_2O_2 into • OH by a Fenton-like reaction. Both in vitro and in vivo experiments have proven that GSH depletion enhanced CDT/NIR-II PTT synergistic therapy based on CuPW@PANI Nanorods induces the effective ablation of tumors. Hence, this work provides an option to develop a simple and multifunctional nanomedicine to realize GSH depletion, • OH production, and NIR-II PTT for effective tumor ablation.

Materials and Methods

The Preparation of Copperphosphotungstate Doped Polyaniline Nanorods

In a typical synthesis procedure of CuPW@PANI Nanorods: aniline (92μL), phosphotungstic acid (188mg), $CuSO_4$ (16 mg), and PVP (200 mg) were added in 18 mL DI water to obtain solution A, which was kept at 5°C. $(NH_4)_2S_2O_3$ (228mg) was added into 10mL DI water to obtain solution B, which was kept at 5 °C. Solution B was drop added into solution A at 5°C

and stirred in 5°C for 4 h at 400 rpm. The blue solution was centrifugated under 5600×g (3000 rpm) to remove large particles for 10 min at room temperature. CuPW@PANI Nanorods were obtained via centrifugation under 18,600×g (11000 rpm) for 10 min at room temperature and extensively washed with DI water and ethanol for several times.

Examining Catalytic Activities of Copperphosphotungstate Doped Polyaniline Nanorods by Detecting ROS, ·OH and GSH Consumption Using DCFH, Methylene Blue or DTNB as Indicator

For all experiments, comparison was made without or with 1064 nm laser irradiation (1.0 W/cm^2, 5 min). For detection of ·OH generation, CuPW@PANI Nanorods (100 μg/mL) were added in 3 mL methylene blue solution (8 μg/mL), followed by stirring for 30 min. Next, 100 μL H_2O_2 (1 mM) was added. After different periods of time, the level of ·OH generation was evaluated based on the decrease of absorbance at 617 nm.

To test the ROS production activity of CuPW@PANI Nanorods, DCFH was used as the probe to detect ^{1}O2 production. Briefly, DCFH-DA (0.5 mL) in DMSO was mixed with NaOH (2mL, 0.01 M) for 30 min. Then PBS (10 mL, 25 mM, pH 7.2) was added to form a stock solution of DCFH-DA. CuPW@PANI Nanorods solution (100μg/mL) was mixed with the stock solution of DCFH-DA (10 μM) with or without H_2O_2 (1 mM). The solutions were placed at room temperature for 2 h. Then the fluorescent spectra were measured to estimate the produced ROS (excitation at 485 nm and emission at 528 nm).

To test GSHOD activity of CuPW@PANI Nanorods, GSH (10 mM, 30 μL) and CuPW@PANI Nanorods (100 μg/mL) were added into PBS solution (1 mL) with or without H_2O_2 (1 mM) at room temperature. After incubation for 30 min at room temperature, DTNB (Ellman's Reagent, (5,5-dithio-bis-(2-nitrobenzoic acid)) solution (3mg/mL, 200 μL) was added and further incubated for 10 min. Oxidation of GSH was quantified by the decrease of absorbance at 412 nm using UV-vis spectroscopy.

Detecting Intracellular ROS and GSH

ROS production was probed by a cell-permeable dye (2,7-dichlorofluorescin diacetate, DCFH-DA), which becomes green fluorescent upon being oxidized to DCF by intracellular ROS. Specifically, 4T1 cells were first seeded in 12-well plates (2 × 104 cells per well) and then cultured for 24 h. Subsequently, the culture medium was replenished and added with DCFH-DA (10 nM). After 20 min, cells were washed thrice with PBS to remove free dyes. Finally, the fluorescence was recorded at 545 nm under 485 nm excitation.

The intracellular GSH was measured by the GSH and GSSG Assay Kit (Beyotime). 4T1cells were seeded in 6-well plates (3 × 10^6 cells per well) and incubated for 24 h. Then, the culture media were replaced with media containing CuPW@PANI Nanorods (100 μg/mL). After 4 h, each well was replaced with the fresh media containing 10% FBS and the cells were incubated for another 20 h. Then, the cells were collected for GSH and GSSG assay according to the manufacturer's protocol.

Results and Discussion

Synthesis and Characterization of Copperphosphotungstate Doped Polyaniline Nanorods

CuPW@PANI Nanorods were synthesized by oxidative chemical polymerization of aniline under phosphotungstic acid, copper (II) sulfate, and ammonium persulphate. In a typical synthetic process, $CuSO_4$, phosphotungstic acid and aniline were mixed with PVP, then ammonium persulphate was added to initiate the polymerization. The reaction was carried out at 5°C for 4h. The mixtures were centrifugated to obtain small blue CuPW@PANI Nanorods.

As exhibited in Figures 1A and S1, the rod-like morphology of CuPW@PANI Nanorods with an axial length of about 180 nm was confirmed by the transmission electron microscopy (TEM) images. The hydrodynamic diameter of the as-designed CuPW@PANI Nanorods was verified to be 185 nm, which was consistent with the TEM examination (Figure 1B). Furthermore, the zeta potential of CuPW@PANI Nanorods was determined to be 36.3 mV. Moreover, negligible change in the particle size of CuPW@PANI Nanorods was observed over 14 days (Figure S2). The biodegradation property of

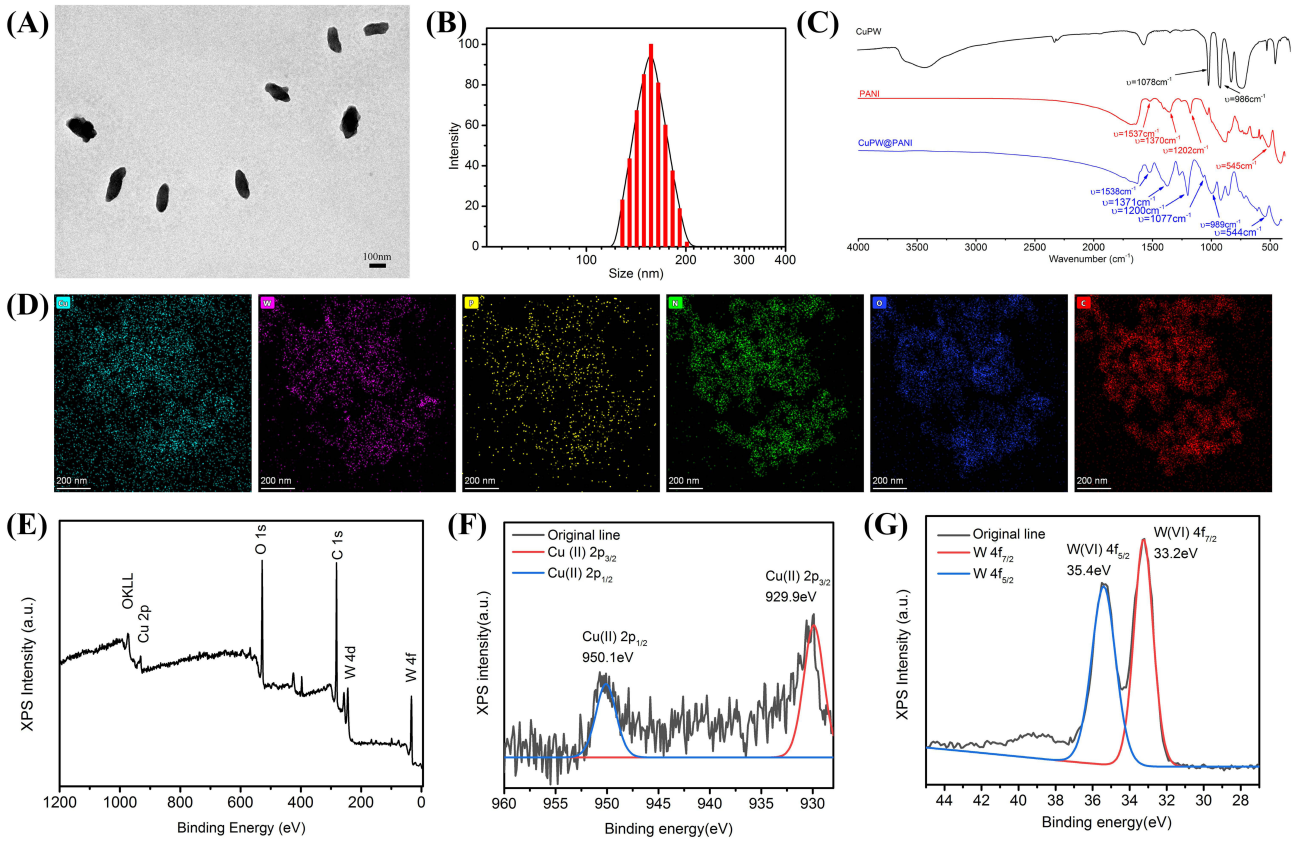

Figure 1 Characterizations of CuPW@PANI Nanorods. (**A**) The TEM of CuPW@PANI Nanorods. (**B**) The DLS of CuPW@PANI Nanorods. (**C**) The IR spectrum of $CuPWO_4$, PANI, CuPW@PANI Nanorods. (**D**) Elemental mapping of Cu, W, P, C, N, and O in CuPW@PANI Nanorods. (**E**) The XPS of CuPW@PANI Nanorods. (**F**) High-resolution XPS spectra of Cu 2p in CuPW@PANI Nanorods. (**G**) High-resolution XPS spectra of W 4f in CuPW@PANI Nanorods.

CuPW@PANI Nanorods after incubation in various pH solutions (pH =5.0, 6.0, and 7.4) was evaluated by ICP-OES investigation. No apparent release of Cu and W could be observed after 7 days under neutral or acidic condition (Table S1). Apart from that, the morphological change of CuPW@PANI Nanorods under acid milieus was also investigated. As demonstrated in Figure S3, CuPW@PANI Nanorods still preserved the rod-like morphology under acid conditions for long-term. All these results confirmed the excellent stability of CuPW@PANI Nanorods in the physiological medium.

The formatted coordination bonds of CuPW@PANI Nanorods were further investigated via Fourier transform infrared (FTIR) spectroscopy. As shown in Figure 1C, the peaks of CuPW@PANI Nanorods which were located at 1537, 1371, 1200, and 544 cm^{-1} were attributed to the bonds from polyaniline. Besides, the band at 1077 and 989 cm^{-1} of CuPW@PANI Nanorods were attributed to copperphosphotungstate. The chemical composition of CuPW@PANI Nanorods was also verified via energy-dispersive X-ray spectroscopy (EDS) elemental mapping. As shown in Figure 1D and E, CuPW@PANI Nanorods consisted of Cu, P, W, O, and N elements, proving the uniform distribution between CuPW and PANI. The atomic composition was also confirmed by X-ray photoelectron spectroscopy (XPS) (Figure 1F and G). According to the well-resolved peaks in Figure 1F, the peaks at 953.3 eV (Cu 2p1/2) and 932.4 eV (Cu 2p3/2) were ascribed to the chemical state of Cu (II). In addition, the two strong peaks at 35.1 eV (W 4f7/2) and 33.2 eV (W 4f5/2) were relevant with the W(VI) valence state. All these results strongly proved the successful fabrication of CuPW@PANI Nanorods.

NIR-II Photothermal Conversion Performance of Copperphosphotungstate Doped Polyaniline Nanorods

The UV-vis-NIR spectra of CuPW@PANI Nanorods in water at different concentrations were investigated. CuPW@PANI Nanorods demonstrated the absorption arranged from 600 to 1100 nm (Figure 2A). The absorbance of CuPW@PANI Nanorods exhibited a linear increase with the increment of concentration. The mass extinction coefficient

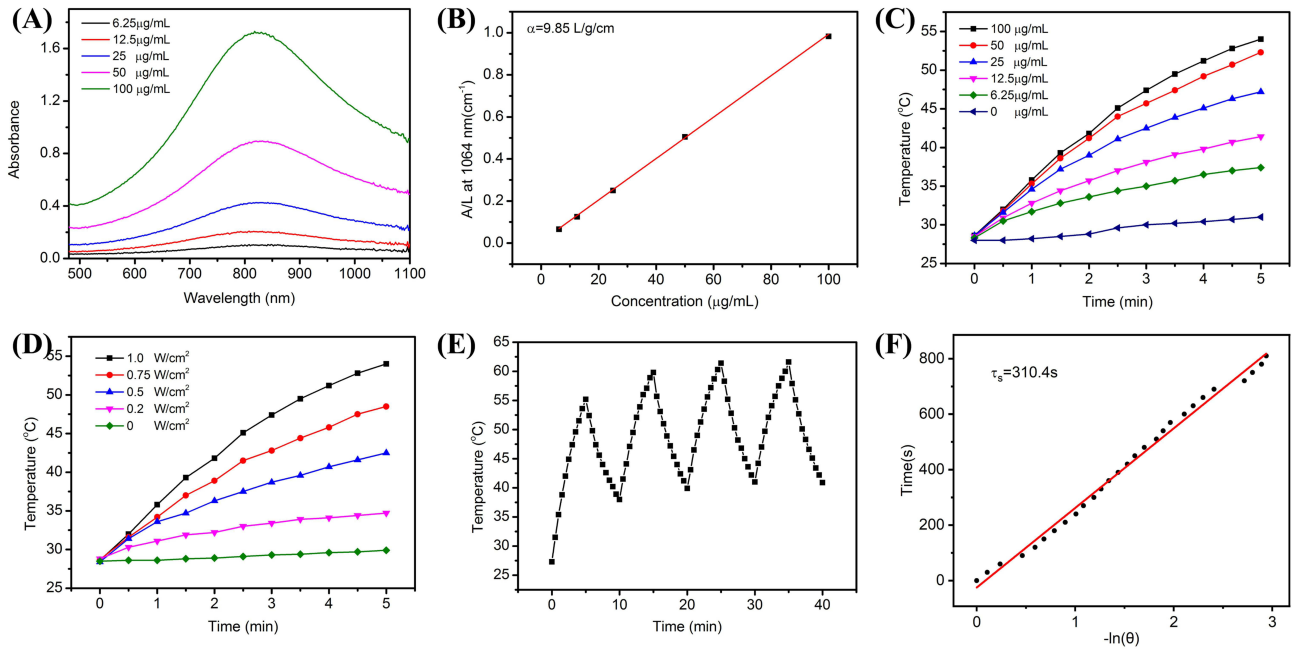

Figure 2 NIR-IIPhotothermal performance of CuPW@PANI Nanorods. (**A**) UV-vis-NIR spectra of CuPW@PANI Nanorods in water with various concentration. (**B**) Fitting curve of mass extinction coefficient of CuPW@PANI Nanorods at 1064 nm. (**C**) Photothermal curves of CuPW@PANI Nanorods with various concentrations (0~100 μg/mL) under 1064 nm laser irradiation (1.0 W/cm^2). (**D**) Temperature elevation curves of CuPW@PANI Nanorods (100 μg/mL) under 1064 nm laser irradiation with different power densities. (**E**) Temperature curves of CuPW@PANI Nanorods after five heating/cooling cycles. (**F**) Linear time constant calculated from the cooling period.

at 1064 nm was determined to be 9.85 L/g.cm, which was much higher than those of TiO_{2-x} (5.54 L/g.cm)[61] and $SrCuSi_4O_{10}$ nanosheets (2.42 L/g.cm)[62] (Figure 2B). It seems that CuPW@PANI Nanorods could efficiently collect and convert NIR-II light energy into hyperthermia.

To explore the photothermal-conversion capability of CuPW@PANI Nanorods, the temperature variation and corresponding images of CuPW@PANI Nanorods at different concentrations after exposure to 1064 nm laser were explored (Figures 2C and D and S4). For example, the temperature of CuPW@PANI Nanorods aqueous solution (100 μg/mL) increased from room temperature to 55°C after irradiation (1064 nm, 1.0 W/cm^2, 5 min). On the contrary, a slight temperature elevation was observed in the water under the same condition, indicating that CuPW@PANI Nanorods exhibited excellent capacity to transfer NIR-II light energy into thermal energy.

Moreover, the photothermal property of CuPW@PANI Nanorods in water was nearly unchanged after five heating/cooling cycles (Figure 2E), confirming the excellent thermal stability of CuPW@PANI Nanorods. Furthermore, to assess the photothermal stability of CuPW@PANI Nanorods, the UV-vis-NIR spectra of CuPW@PANI Nanorods aqueous solution were explored after continuous 1064 nm laser irradiation. As shown in Figure S5, the UV-vis-NIR spectra of CuPW@PANI Nanorods remained unchanged after 1064 nm laser irradiation for 30 min. All these results confirmed the high photothermal stability of CuPW@PANI Nanorods.

As shown in Figure 2F, the photothermal-conversion efficiency of CuPW@PANI Nanorods was determined to be 45.14%, which is high compared with most of the other NIR-II PTT agents, such as the gold nanoframeworks (23.9%),[63] semiconducting copolymer nanoparticles (43.4%),[64] MoS_2 nanomaterials (43.3%).[43] Therefore, all these results verified that CuPW@PANI Nanorods are optional for NIR-II photothermal therapy.

The GSH Depletion and ROS Generation of Copperphosphotungstate Doped Polyaniline Nanorods

The GSH depletion performance of CuPW@PANI Nanorods was exploited using the DTNB as a GSH indicator. After incubation with CuPW@PANI Nanorods, the GSH concentrations were investigated for various durations. As shown in

Figure S6, the absorption of DNTB changed slightly, confirming the stability of GSH. As depicted in Figure 3A, the GSH concentrations decreased gradually as incubation time increased. XPS analysis was carried out to verify the oxidation-reduction reaction between CuPW@PANI Nanorods and GSH (Figure 3B). The emergence of Cu^{+} and the weakening of Cu^{2+} in the valence state of Cu proved the reduction of copper. In addition, the valence state of W keeps stable (Figure S7). The existence of Cu^{2+}/Cu^{+} couples endow CuPW@PANI Nanorods with GSH depletion property (Figure 3F).

CuPW@PANI Nanorods were speculated to catalyze H_2O_2 and generate •OH. Therefore, the Fenton-like reaction activity of CuPW@PANI Nanorods was validated by using the 3,3,5,5-tetramethyl-benzidine (TMB) as indicator. As depicted in Figure S8, with the increment of CuPW@PANI Nanorods concentration, the absorbance value of TMB at 652 nm significantly increases, indicating the production of •OH. In the presence of H_2O_2, the production of •OH by CuPW@PANI Nanorods was also confirmed with the methylene blue (MB) discoloration experiment. Figure 3C shows the absorption changes of MB after different treatments. The absorbance intensity of MB treated with H_2O_2, CuPW@PANI Nanorods or CuPW@PANI Nanorods +1064nm was negligible. On the contrary, CuPW@PANI Nanorods + H_2O_2 groups exhibited apparent absorbance at 617nm, indicating that CuPW@PANI Nanorods have Fenton-like reaction activity. Moreover, the absorbance at 617 nm of CuPW@PANI Nanorods + H_2O_2 after 1064 nm irradiation was stronger compare to that without 1064 nm irradiation, confirming that photothermal treatment could improve the Fenton-like reaction activity. Simultaneously, the Fenton-like reaction activity of CuPW@PANI Nanorods increased with the increment of H_2O_2 concentration (Figure S9). It seems that higher H_2O_2 concentration results in faster MB degradation.

Figure 3D shows the fluorescent changes of DCF after different treatments. As can be seen in Figure 3D, different fluorescent intensity after various treatments were observed. The fluorescent signal in the group treated with H_2O_2, CuPW@PANI Nanorods or CuPW@PANI Nanorods +1064nm was negligible. On the contrary, the CuPW@PANI Nanorods + H_2O_2 groups exhibited a fluorescent signal at 450nm, indicating that CuPW@PANI Nanorods have Fenton-like reaction activity. Moreover, the enhanced fluorescent signal was observed in the CuPW@PANI Nanorods + H_2O_2 with a 1064nm irradiation group, confirming that photothermal treatment could improve the Fenton-like reaction efficacy.

The generation of •OH was further exploited by electron spinning resonance (ESR) spectra with 5,5-dimethyl-1-pyrroline N-oxide (DMPO) as •OH trapping agent. As demonstrated in Figure 3E, CuPW@PANI Nanorods alone, H_2O_2 alone, and CuPW@PANI Nanorods plus 1064 nm irradiation could not lead to the production of •OH. After

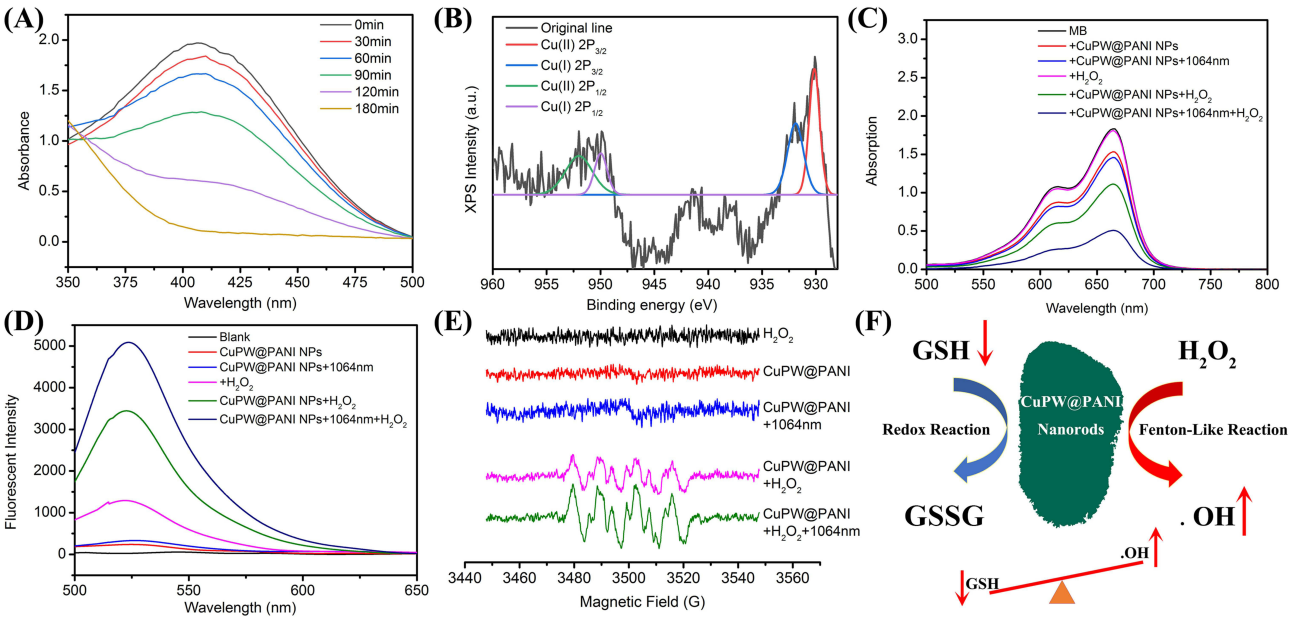

Figure 3 Characterizations of the redox and Fenton-like reaction of CuPW@PANI Nanorods. (**A**) GSH depletion by CuPW@PANI Nanorods with DTNB as indicator after different duration. (**B**) XPS spectrum of CuPW@PANI Nanorods after reaction with GSH. (**C**) MB degradation by .OH generated by H_2O_2 and CuPW@PANI Nanorods at different groups. (**D**) Fluorescent spectrum of DCF for ROS generation. (**E**) ESR spectrum after different treatment. (**F**) The illustration of the GSH depletion and Fenton-like performance of CuPW@PANI Nanorods (Up red arrow means the generation of .OH, while the down red arrow means the depletion of GSH).

combination CuPW@PANI Nanorods with H_2O_2, an apparent ESR signal was monitored. Moreover, the ESR signal intensity after 1064 nm irradiation was enhanced, which was consistent with the MB degradation experiments. Therefore, all the results confirmed that CuPW@PANI Nanorods could produce toxic •OH to kill tumor cells (Figure 3F).

In a word, we designed copperphosphotungstate doped polyaniline nanorods to induce the GSH consumption enhanced Fenton-like reaction and NIR-II PTT, having the great potential to augment tumor therapy.

In vitro Therapeutic Efficacy Assessment of Copperphosphotungstate Doped Polyaniline Nanorods

Encouraged by the physicochemical properties and functions of CuPW@PANI Nanorods, in vitro experiments were carried out to investigate the therapeutic efficacy. CuPW@PANI Nanorods exhibited no apparent toxicity to normal cells (L929) whereas they were cytotoxic to tumor cells (4T1) with the increment of concentration (Figure 4A), due to the higher endogenous H_2O_2 in tumor cells than that in normal cells. The anti-tumor effect was greatly improved by 1064 nm irradiation or the addition of H_2O_2 incorporation with CuPW@PANI Nanorods (Figures 4B and S10). For example, after treatment with CuPW@PANI Nanorods (100 μg/mL) and H_2O_2 (200 μM), the enhancement of cytotoxicity was observed and more than 50% death of 4T1 cells was recorded. Moreover, with 100 μg/mL CuPW@PANI Nanorods, 1064 nm irradiation (0.75 W/cm^2, 3 min) plus 200μM extracellular H_2O_2, essentially 94% 4T1 cells were killed. This was ascribed to the GSH depletion by CuPW@PANI Nanorods, the abundant generation of •OH via the Fenton-like reaction incorporated with NIR-II photothermal therapy.

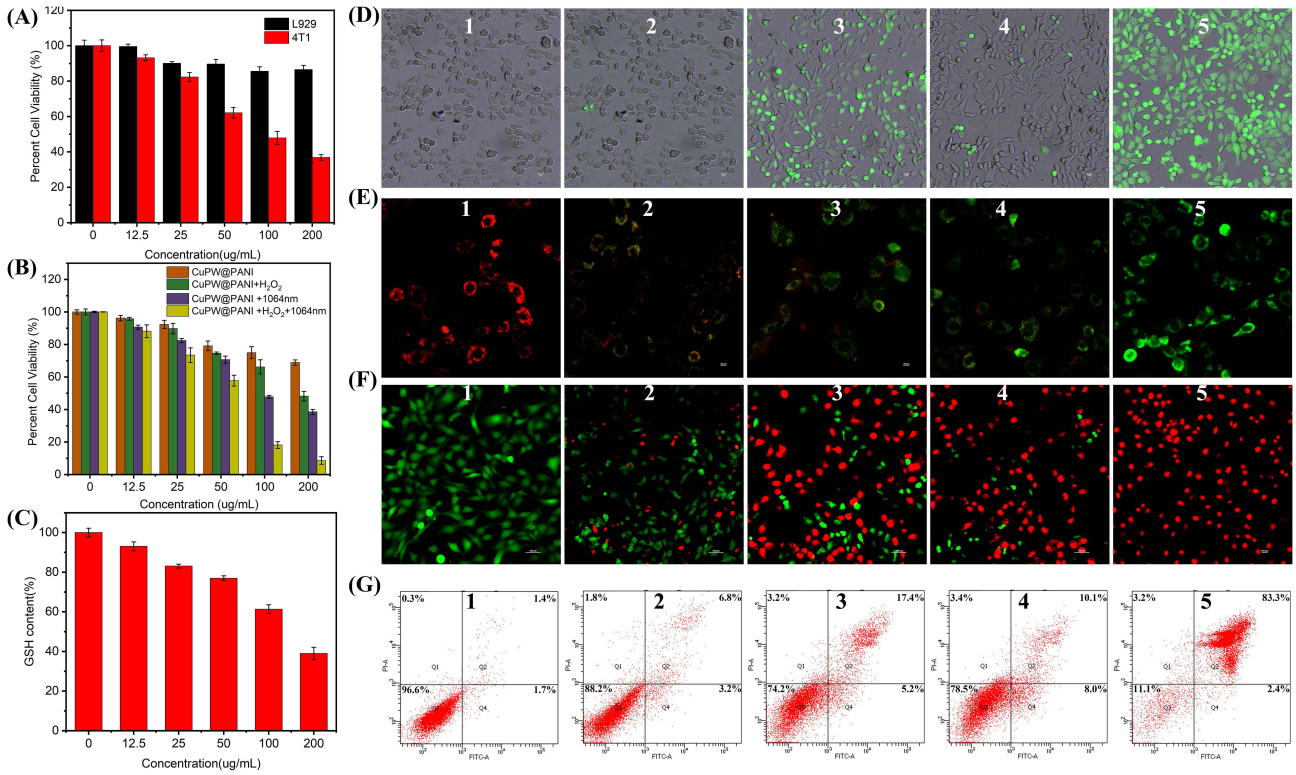

Figure 4 Intracellular investigation of CuPW@PANI Nanorods. (**A**) Cytotoxicity of L929 and 4T1 cells after incubation with CuPW@PANI Nanorods for 24h. (**B**) 4T1 cells viability after treatment with CuPW@PANI Nanorods for 4h, then in presence or absence of H_2O_2 (100 μM) with or without 1064nm irradiation (0.75 W/cm^2, 5 min). (**C**) GSH depletion in cells after incubation with CuPW@PANI Nanorods (0 to 200 μg/mL). (**D**) Fluorescence images of 4T1 cells after different treatment stained by DCFH-DA. (**E**) Fluorescence images of 4T1 cells after different treatment stained by JC-1. (**F**) Fluorescent images of 4T1 cells after different treatment and then stained by PI and Ca-AM. (**G**) Flow cytometry using Annexin-V-FTIC/PI assay of 4T1 cells after different treatment. In the (**D**–**G**), 1. 4T1 cells treated with PBS, 2. 4T1 cells treated with CuPW@PANI Nanorods (100μg/mL), 3. 4T1 cells treated with CuPW@PANI Nanorods (100μg/mL) and H_2O_2(100μM), 4. 4T1 cells treated with CuPW@PANI Nanorods (100μg/mL) plus NIR-II irradiation (1064 nm laser, 0.75 W/cm^2, 5 min), 5. 4T1 cells treated with CuPW@PANI Nanorods (100μg/mL) and H_2O_2(100μM) plus NIR-II irradiation (1064 nm laser, 0.75 W/cm^2, 5 min).

Owing to copperphosphotungstate which could oxidize GSH, it is supposed that intracellular GSH could be consumed by CuPW@PANI Nanorods. Hence, the GSH level in tumor cells after treatment with CuPW@PANI Nanorods was further investigated. As demonstrated in Figure 4C, the reduction of GSH level in 4T1 cells was observed after incubation with CuPW@PANI Nanorods, which could be attributed to the copperphosphotungstate-mediated oxidation.

To explore ROS production in vitro, DCFH-DA was utilized as the probe. As displayed in Figure 4D, a negligible green fluorescence was observed from the PBS or CuPW@PANI Nanorods alone group. 4T1 cells treated with CuPW@PANI Nanorods plus 1064 nm irradiation exhibited weak green fluorescence due to the finite •OH production. Interestingly, in the presence of H_2O_2, strong green fluorescence was observed in CuPW@PANI Nanorods group, implying the generation of •OH. Notably, 4T1 cells presented conspicuous green fluorescence image after treated with CuPW@PANI and H_2O_2 under 1064 nm irradiation. It seems that the hydroxyl radical generation ability of CuPW@PANI Nanorods could be enhanced with NIR-II laser-induced hyperthermia.

To investigate the dysfunction of mitochondria after different treatment, the JC-1 staining experiment was carried out to explore the mitochondrial membrane potential. As demonstrated in Figure 4E, only the red fluorescence could be detected in the PBS group, confirming the no change in mitochondrial membrane potential. Only a slightly enhanced green fluorescence was observed in 4T1 cells after treatment with CuPW@PANI Nanorods, whereas the modest fluorescent ratio between the green with red could be detected in the group (CuPW@PANI Nanorods plus 1064 nm irradiation) and group (CuPW@PANI Nanorods and H_2O_2), confirming the damage of mitochondria. To our surprise, only the green fluorescence was observed in the group (CuPW@PANI Nanorods+ H_2O_2 + 1064 nm laser), indicating the damage of abundant mitochondria. These results evidently prove that the local hyperthermia generated from CuPW@PANI Nanorods with 1064 nm irradiation plus the CDT might kill efficiently tumor cell.

Next, the Calcein-AM and PI assay was used to investigate the cell apoptosis. As demonstrated in Figure 4F, only CuPW@PANI Nanorods could not result in noticeable cell death. However, after treatment with CuPW@PANI Nanorods and H_2O_2, evident cell death was observed through the depletion of GSH and chemodynamic combination therapy. Moreover, CuPW@PANI Nanorods plus 1064nm irradiation could also result in cell death, which was ascribed to the NIR-II laser-induced hyperthermia. As expected, after CuPW@PANI Nanorods and H_2O_2 plus 1064nm irradiation, the optimal therapeutic effect was achieved through the GSH depletion, •OH generation, and hyperthermia combination therapy.

The quantitative analysis based on flow cytometry further demonstrated that the proportions of apoptotic cells were 1.4%, 6.8%, 17.4%, 10.4%, and 83.3% in the cells after being treated by PBS, CuPW@PANI Nanorods, CuPW@PANI Nanorods + 1064 nm laser, CuPW@PANI Nanorods +H_2O_2, and CuPW@PANI Nanorods +H_2O_2 +1064 nm laser, respectively (Figure 4G). This result was in accordance with the Calcein-AM/PI and CCK-8 results and confirmed the interaction between CuPW@PANI Nanorods and tumor cells. All these results confirmed that CuPW@PANI Nanorods own outstanding GSH depletion enhanced CDT/NIR-II PTT for tumor elimination.

In vivo Biocompatibility and Biodistribution Assessment of Copperphosphotungstate Doped Polyaniline Nanorods

The biocompatibility of CuPW@PANI Nanorods was investigated for latent therapeutic application. The BALB/C mice were intravenously injected with various doses of CuPW@PANI Nanorods (0, 10, 20, and 40 mg/kg). The body weights of all the mice were recorded every 4 days, and negligible weight change was observed in all groups (Figure S11). Moreover, routine blood chemistry analysis was carried out postinjection of CuPW@PANI Nanorods. As depicted in Figure S12, no significant difference in blood indexes of the mice in all groups was detected. Furthermore, hematoxylin and eosin (H&E) staining experiments of the main organs in all groups were performed to assess the histocompatibility of CuPW@PANI Nanorods. As demonstrated in Figure S13, there are no significant pathological abnormalities or inflammatory lesions in all groups. All these results proved that CuPW@PANI Nanorods possess satisfactory biocompatibility for further therapeutic utility.

Inspired by the desirable NIR-II absorption, the potential of CuPW@PANI Nanorods as photoacoustic (PA) imaging agents was evaluated. The PA signals and imaging of CuPW@PANI Nanorods in water with various concentrations were

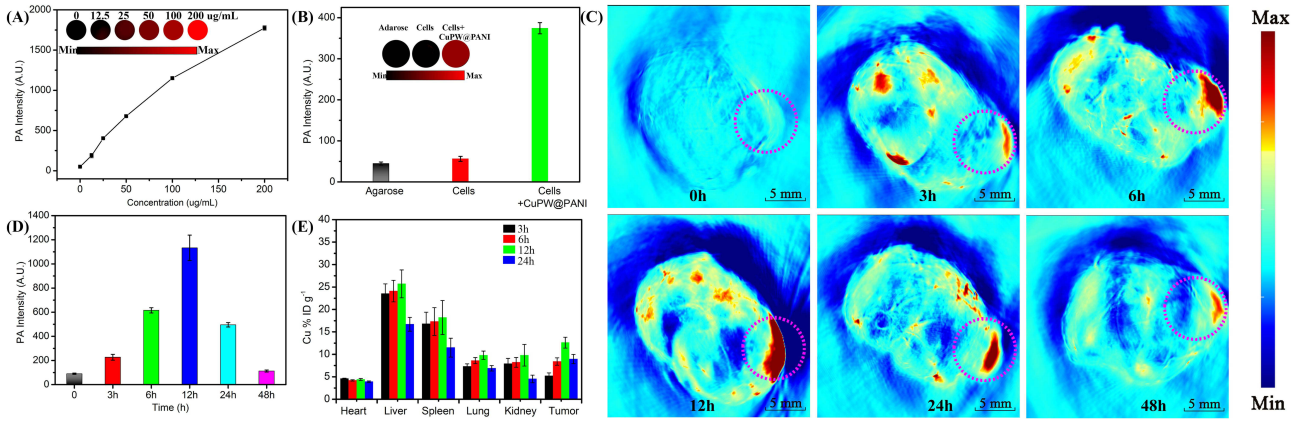

Figure 5 The Biodistribution of CuPW@PANI Nanorods (**A**) The PA intensity and imaging of CuPW@PANI Nanorods with different concentration. (**B**) The PA intensity and imaging of 4T1 cells incubated with or without CuPW@PANI Nanorods. (**C**) The PA imaging of 4T1-bearing mice after injection of CuPW@PANI Nanorods (The tumor area was marked with pink circle). (**D**) The quantity analysis of PA intensity in tumor after injection of CuPW@PANI Nanorods. (**E**) The Cu concentration in different organic tissues after injection of CuPW@PANI Nanorods.

recorded. As displayed in Figure 5A, the PA signal intensity enhanced with the increment of CuPW@PANI Nanorods concentrations in the range of 0~200μg/mL. Moreover, the enhanced PA signal was detected in the 4T1 cells after incubation with CuPW@PANI Nanorods (Figure 5B). Furthermore, after intravenous injection of CuPW@PANI Nanorods, PA imaging of 4T1 breast tumor-bearing mice were carried out (Figure 5C and D). The maximum PA signal at tumor region at 12 h after injection was recorded. Therefore, CuPW@PANI Nanorods featured high potential for PA imaging-guided CDT/NIR-II PTT.

Before assessing the therapeutic effect in vivo, the biodistribution of CuPW@PANI Nanorods in 4T1 tumor-bearing mice was evaluated. The major organs and tumor tissues were gathered at 3, 6, 12, and 24 h after intravenous injection of CuPW@PANI Nanorods, and the content of the Cu element was determined. As displayed in Figure 5E, the highest tumor accumulation of the composite was observed at 12 h postinjection in consonance with the PA imaging experiment. Moreover, obvious distribution was also observed in liver, spleen, and kidney due to the blood circulation and the capture of reticuloendothelial system. Based on the consequences of PA imaging and the biodistribution examination, the NIR-II photothermal therapy was carried out at 12h after injection of CuPW@PANI Nanorods via the tail vein.

In vivo Synergistic CDT/NIR-II PTT Performance of Copperphosphotungstate Doped Polyaniline Nanorods

To further explore the in vivo therapeutic effect of CuPW@PANI Nanorods, thirty mice bearing 4T1 tumor were randomly divided into five groups (PBS, CuPW@PANI Nanorods, CuPW@PANI Nanorods +1064 nm laser, CuPW@PANI Nanorods+H_2O_2, and CuPW@PANI Nanorods +H_2O_2+1064 nm laser). The tumor regions were irradiated by the 1064 nm laser at 12h after intravenous injection of CuPW@PANI Nanorods. The temperature and thermal images of the tumor sites were recorded by a thermal imaging camera (Figure 6A and B). The temperature at the tumor site in the group treated by CuPW@PANI Nanorods + 1064 nm laser elevated quickly and reached 50.5°C within 5 min, confirming the high photothermal capability of CuPW@PANI Nanorods. On the contrary, a slight temperature increase (3°C) in the tumor region was detected in the control groups (PBS+1064 nm laser).

After various treatments, the tumor volumes and body weights of mice in all groups were recorded every 2 days. There are no significant weight loss in all groups, suggesting the high biosafety of CuPW@PANI Nanorods (Figure 6C). As shown in Figure 6D, little tumor inhibition could be observed in the PBS group or CuPW@PANI Nanorods group. To our surprise, the CuPW@PANI Nanorods +1064nm group or CuPW@PANI Nanorods +H_2O_2 group exhibited moderate tumor suppression, suggesting NIR-II PTT or CDT alone cannot efficiently inhibit tumor. Furthermore, synergistic therapy of NIR-II PTT and CDT significantly inhibited tumor, confirming the superior therapeutic effect of CDT/NIR-II PTT combination therapy compared to NIR-II PTT or CDT alone. Moreover, the digital photography and tumor

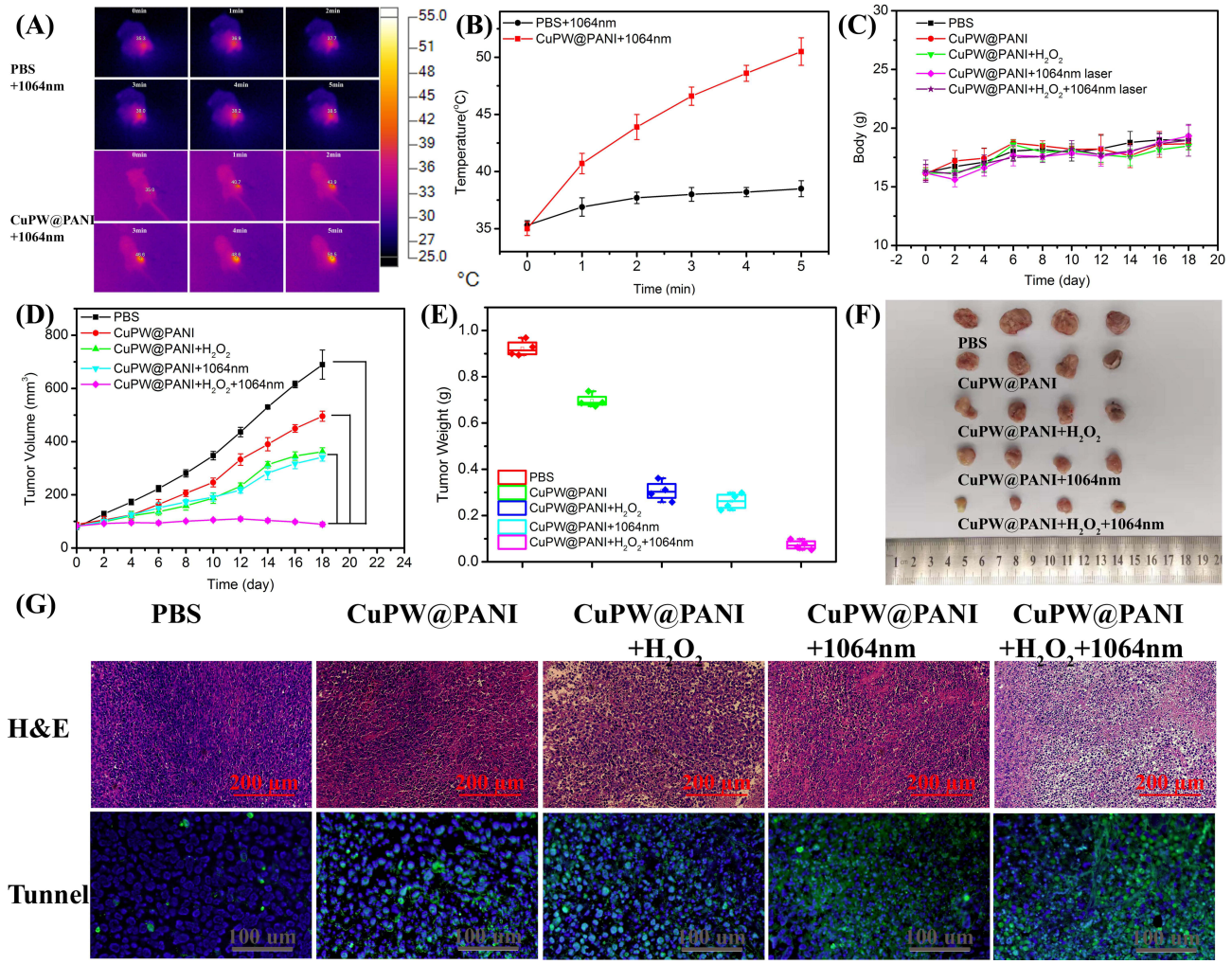

Figure 6 The therapeutic effect of CuPW@PANI Nanorods. (**A**) Photothermal images of 4T1 tumor-bearing mice administration with PBS (control) or CuPW@PANI Nanorods after 1064 nm laser irradiation (0.75 W/cm^2) for different durations. (**B**) The temperature of tumor sites change. (**C**) The body weight of mice after different treatments. (**D**) Growth curves of tumors in 4T1 tumor-bearing mice after different treatments. (**E**) Tumor weight after different treatments. (**F**) The photo of tumor after different treatments. (**G**) H&E and Tunnel staining of tumors with different treatments.

weights also proved the most tumor suppression in "combination therapy" group (Figure 6E and F). All these results confirmed the higher therapeutic effect of NIR-II PTT plus CDT, compare to NIR-II PTT or CDT alone.

H&E staining of tumor tissues were also carried out to assess the therapeutic efficacy in all groups (Figure 6G). There is modesty necrosis with deformed nuclei in the CuPW@PANI Nanorods + 1064 nm or CuPW@PANI Nanorods +H_2O_2 group, compared to the PBS group. Moreover, most serious necrosis with distorted nuclei was detected in the CuPW@PANI Nanorods + 1064 nm +H_2O_2 group. Then, the Tunnel staining of tumor tissues in all groups were performed to evaluate apoptosis of tumor cells after different treatment (Figure 6G). The proportion of proliferation tumor cells in the CuPW@PANI Nanorods + 1064 nm group or CuPW@PANI Nanorods +H_2O_2 group decreased, respectively, while the percentage of apoptotic cells increased after administration of CuPW@PANI Nanorods + 1064 nm +H_2O_2. These results proved that CDT/NIR-II PTT combination therapy could inhibit tumor and induce tumor cell apoptosis.

Conclusion

In general, we fabricated a novel copperphosphotungstate doped polyanilines nanorods (CuPW@PANI Nanorods) to disrupt the redox homeostasis in tumor cells. CuPW@PANI Nanorods featured strong NIR-II absorbance and high

photothermal-conversion efficiency (45.14%). Moreover, CuPW@PANI Nanorods were characterized to consume GSH and convert H_2O_2 into • OH by a Fenton-like reaction. Both in vitro and in vivo experiments have confirmed that GSH depletion enhanced CDT/NIR-II PTT synergistic therapy based on CuPW@PANI Nanorods could effectively ablate tumors. Consequently, this work provides an alternative but efficient avenue to surmount the drawbacks of GSH depletion enhanced CDT via combination NIR-II PTT for effective cancer treatment.

Abbreviations

CuPW, CopperPhosphotungstate; CuPW@PANI, CopperPhosphotungstate doped Polyanilines; H_2O_2, Hydrogen Peroxide; CDT, ChemodynamicTherapy; PPT, Photothermal Therapy; PANI, Polyanilines; TME, Tumor Microenvironment; ROS, Reactive Oxygen Species; MPE, Maximum Permissible Exposure; TMB, 3,3,5,5-Tetramethyl-Benzidine; TEM, Transmission Electron Microscopy; FTIR, Fourier Transform Infrared; XPS, X-ray Photoelectron Spectroscopy; ESR, Electron Spinning Resonance.

Ethics Approval and Consent to Participate

Animal experiment is in accordance with the regulations of the Animal Ethical and Welfare Committee of Southern Medical University (SYXK2016-0167).

Author Contributions

All authors made a significant contribution to the work reported, whether that is in the conception, study design, execution, acquisition of data, analysis and interpretation, or in all these areas; took part in drafting, revising or critically reviewing the article; gave final approval of the version to be published; have agreed on the journal to which the article has been submitted; and agree to be accountable for all aspects of the work.

Funding

We gratefully acknowledge the National Natural Science Foundation of China (81671749) for financial support.

Disclosure

The authors declare no competing interests in the paper.

References

1. Ray PD, Huang BW, Tsuji Y. Reactive oxygen species (ROS) homeostasis and redox regulation in cellular signaling. *Cell Signal*. 2012;24(5):981–990.
2. Tretter V, Hochreiter B, Zach ML, Krenn K, Klein KU. Understanding cellular redox homeostasis: a challenge for precision medicine. *Int J Mol Sci*. 2022;23(1):106. doi:10.3390/ijms23010106
3. Marengo B, Nitti M, Furfaro AL, et al. Redox homeostasis and cellular antioxidant systems: crucial players in cancer growth and therapy. *Oxid Med Cell Longev*. 2016;2016:6235641.
4. Yang BW, Chen Y, Shi JL. Reactive oxygen species (ROS)-based nanomedicine. *Chem Rev*. 2019;119(8):4881–4985.
5. Sies H, Jones DP. Reactive oxygen species (ROS) as pleiotropic physiological signalling agents. *Nat Rev Mol Cell Biol*. 2020;21(7):363–383.
6. Shah A, Rogoff HA. Implications of reactive oxygen species on cancer formation and its treatment. *Semin Oncol*. 2021;48(3):238–245.
7. Wang Y, Qi H, Liu Y, et al. The double-edged roles of ROS in cancer prevention and therapy. *Theranostics*. 2021;11(10):4839–4857.
8. Prasad S, Gupta SC, Tyagi AK. Reactive oxygen species (ROS) and cancer: role of antioxidative nutraceuticals. *Cancer Lett*. 2017;387:95–105.
9. Nishikawa M. Reactive oxygen species in tumor metastasis. *Cancer Lett*. 2008;266(1):53–59.
10. Lennicke C, Rahn J, Lichtenfels R, Wessjohann LA, Seliger B. Hydrogen peroxide-production, fate and role in redox signaling of tumor cells. *Cell Commun Signal*. 2015;13(1):1–19. doi:10.1186/s12964-015-0118-6
11. Jeronimo A, Rodrigues G, Vilas-Boas F, Martins GG, Bagulho A, Real C. Hydrogen peroxide regulates angiogenesis-related factors in tumor cells. *Biochem Cell Biol*. 2017;95(6):679–685. doi:10.1139/bcb-2017-0083
12. Bansal A, Simon MC. Glutathione metabolism in cancer progression and treatment resistance. *J Cell Biol*. 2018;217(7):2291–2298. doi:10.1083/jcb.201804161
13. Singh S, Khan AR, Gupta AK. Role of glutathione in cancer pathophysiology and therapeutic interventions. *J Exp Ther Oncol*. 2012;9(4):303–316.
14. Tang ZM, Liu YY, He MY, Bu WB. Chemodynamic therapy: tumour microenvironment-mediated Fenton and Fenton-like reactions. *Angew Chem Int Edit*. 2019;58(4):946–956. doi:10.1002/anie.201805664
15. Jia CY, Guo YX, Wu FG. Chemodynamic therapy via Fenton and Fenton-like nanomaterials: strategies and recent advances. *Small*. 2022;18(6):2103868. doi:10.1002/smll.202103868
16. Xin JQ, Deng CT, Aras O, Zhou MJ, Wu CS, An FF. Chemodynamic nanomaterials for cancer theranostics. *J Nanobiotechnol*. 2021;19(1):1–26.

17. Paolicchi A, Dominici S, Pieri L, Maellaro E, Pompella A. Glutathione catabolism as a signaling mechanism. *BiochemPharmacol*. 2002;64(5–6):1027–1035.
18. Franco R, Cidlowski JA. Glutathione efflux and cell death. *Antioxid Redox Signal*. 2012;17(12):1694–1713.
19. Lash LH. Renal glutathione transport: identification of carriers, physiological functions, and controversies. *Biofactors*. 2009;35(6):500–508. doi:10.1002/biof.65
20. Lu SC. Glutathione synthesis. *Biochim Biophys Acta Gen Subj*. 2013;1830(5):3143–3153. doi:10.1016/j.bbagen.2012.09.008
21. Zhang HQ, Forman HJ. Glutathione synthesis and its role in redox signaling. *Semin Cell Dev Biol*. 2012;23(7):722–728.
22. Zhou YF, Fan SY, Feng LL, Huang XL, Chen XY. Manipulating intratumoral Fenton chemistry for enhanced chemodynamic and chemodynamic-synergized multimodal therapy. *Adv Mater*. 2021;33(48):2104223.
23. Niu BY, Liao KX, Zhou YX, et al. Application of glutathione depletion in cancer therapy: enhanced ROS-based therapy, ferroptosis, and chemotherapy. *Biomaterials*. 2021;277:121110.
24. Zhang L, Li CX, Wan SS, Zhang XZ. Nanocatalyst-mediated chemodynamic tumor therapy. *Adv Healthc Mater*. 2022;11(2):2101971.
25. Xiong YX, Xiao C, Li ZF, Yang XL. Engineering nanomedicine for glutathione depletion-augmented cancer therapy. *Chem Soc Rev*. 2021;50(10):6013–6041.
26. Cheng XT, Xu HD, Ran HH, Liang GL, Wu FG. Glutathione-depleting nanomedicines for synergistic cancer therapy. *ACS Nano*. 2021;15(5):8039–8068.
27. Yu J, Xiao H, Yang Z, et al. A potent strategy of combinational blow toward enhanced cancer chemo-photodynamic therapy via sustainable GSH elimination. *Small*. 2022;18(9):2106100.
28. Yao JL, Zheng F, Yao CY, et al. Rational design of nanomedicine for photothermal-chemodynamic bimodal cancer therapy. *Wiley Interdiscip Rev Nanomed Nanobiotechnol*. 2021;13(3):e1682.
29. Liu GY, Zhu JW, Guo H, et al. Mo_2C-derived polyoxometalate for NIR-II photoacoustic imaging-guided chemodynamic/photothermal synergistic therapy. *Angew Chem Int Ed*. 2019;58(51):18641–18646.
30. Shan BB, Liu HY, Li LH, Lu YX, Li M. Near-infrared II plasmonic phototheranostics with glutathione depletion for multimodal imaging-guided hypoxia-tolerant chemodynamic-photocatalytic-photothermal cancer therapy triggered by a single laser. *Small*. 2022;18(4):2105638.
31. Chang MY, Wang M, Wang MF, et al. A multifunctional cascade bioreactor based on hollow-structured Cu_2MoS_4 for synergetic cancer chemo-dynamic therapy/starvation therapy/phototherapy/immunotherapy with remarkably enhanced efficacy. *Adv Mater*. 2019;31(51):1905271.
32. Cun JE, Pan Y, Zhang Z, et al. Photo-enhanced upcycling H_2O_2 into hydroxyl radicals by IR780-embedded Fe3O4@MIL-100 for intense nanocatalytic tumor therapy. *Biomaterials*. 2022;287:121687.
33. Li J, Zhang Z, Li J, et al. Copper-olsalazine metal-organic frameworks as a nanocatalyst and epigenetic modulator for efficient inhibition of colorectal cancer growth and metastasis. *Acta Biomater*. 2022;152:495–506.
34. Cun JE, Fan X, Pan Q, et al. Copper-based metal-organic frameworks for biomedical applications. *Adv Colloid Interface Sci*. 2022;305:102686.
35. Xu C, Pu KY. Second near-infrared photothermal materials for combinational nanotheranostics. *Chem Soc Rev*. 2021;50(2):1111–1137.
36. Zhen X, Pu KY, Jiang XQ. Photoacoustic imaging and photothermal therapy of semiconducting polymer nanoparticles: signal amplification and second near-infrared construction. *Small*. 2021;17(6):2004723.
37. Xu WH, Wang D, Tang BZ. NIR-II AIEgens: a win-win integration towards bioapplications. *Angew Chem Int Edit*. 2021;60(14):7476–7487.
38. Jia J, Liu GY, Xu WJ, et al. Fine-tuning the homometallic interface of Au-on-Au nanorods and their photothermal therapy in the NIR-II window. *Angew Chem Int Edit*. 2020;59(34):14443–14448.
39. Xia YN, Li WY, Cobley CM, et al. Gold nanocages: from synthesis to theranostic applications. *Acc Chem Res*. 2011;44(10):914–924.
40. Zhou Z, Li BW, Shen C, et al. Metallic 1T phase enabling MoS_2 nanodots as an efficient agent for photoacoustic imaging guided photothermal therapy in the near-infrared-II window. *Small*. 2020;16(43):2004173.
41. Ling X, Jin ZK, Jiang Q, et al. Engineering biocompatible TeSexnano-alloys as a versatile theranostic nanoplatform. *Natl Sci Rev*. 2021;8(6):nwaa156.
42. Liu ZW, Zhao XY, Yu BR, Zhao NN, Zhang C, Xu FJ. Rough carbon-iron oxide nanohybrids for near-infrared-II light-responsive synergistic antibacterial therapy. *ACS Nano*. 2021;15(4):7482–7490.
43. Han Y, Liu HM, Fan M, et al. Near-infrared-II photothermal ultra-small carbon dots promoting anticancer efficiency by enhancing tumor penetration. *J Colloid Interface Sci*. 2022;616:595–604.
44. Lv RC, Yang PP, He F, et al. A yolk-like multifunctional platform for multimodal imaging and synergistic therapy triggered by a single near-infrared light. *ACS Nano*. 2015;9(2):1630–1647.
45. Dong LL, Li K, Wen D, Gao X, Feng J, Zhang HJ. Engineering gadolinium-integrated tellurium nanorods for theory-oriented photonic hyperthermia in the NIR-II biowindow. *Small*. 2020;16(42):2003508.
46. Cheng L, Wang XW, Gong F, Liu T, Liu Z. 2D nanomaterials for cancer theranostic applications. *Adv Mater*. 2020;32(13):1902333.
47. An D, Fu JY, Zhang B, et al. NIR-II responsive inorganic 2D nanomaterials for cancer photothermal therapy: recent advances and future challenges. *Adv Funct Mater*. 2021;31(32):2101625.
48. Du LH, Qin H, Ma T, Zhang T, Xing D. In vivo imaging-guided photothermal/photoacoustic synergistic therapy with bioorthogonal metabolic glycoengineering-activated tumor targeting nanoparticles. *ACS Nano*. 2017;11(9):8930–8943.
49. Pan HH, Li SK, Kan JL, et al. A cruciform phthalocyanine pentad-based NIR-II photothermal agent for highly efficient tumor ablation. *Chem Sci*. 2019;10(35):8246–8252.
50. Yin C, Li XZ, Wang Y, et al. Organic semiconducting macromolecular dyes for NIR-II photoacoustic imaging and photothermal therapy. *Adv Funct Mater*. 2021;31(37):2104650.
51. Jiang YY, Huang JG, Xu C, Pu KY. Activatable polymer nanoagonist for second near-infrared photothermal immunotherapy of cancer. *Nat Commun*. 2021;12(1):1–14.
52. Zare EN, Makvandi P, Ashtari B, Rossi F, Motahari A, Perale G. Progress in conductive polyaniline-based nanocomposites for biomedical applications: a review. *J Med Chem*. 2020;63(1):1–22.
53. Pina CD, Falletta E. Advances in polyaniline for biomedical applications. *Curr Med Chem*. 2022;29(2):329–357.
54. Zhang Y, Wang YJ, Yang XQ, Yang QL, Li J, Tan WH. Polyaniline nanovesicles for photoacoustic imaging-guided photothermal-chemo synergistic therapy in the second near-infrared window. *Small*. 2020;16(35):2001177.

55. Wang SL, Zhang LL, Zhao JJ, He M, Huang Y, Zhao SL. A tumor microenvironment-induced absorption red-shifted polymer nanoparticle for simultaneously activated photoacoustic imaging and photothermal therapy. *Sci Adv*. 2021;7(12):eabe3588.
56. Kuang YL, Liu NB, Ye S, et al. Ce doped polyaniline nanoparticles for absorption and photoacoustic imaging response to GSH in vitro and in vivo. *Bioact Mater*. 2022;17:197–203.
57. Tian C, Xue XL, Chen Y, et al. Phosphotungstate acid doped polyanilines nanorods for in situ NIR-II photothermal therapy of orthotopic hepatocellular carcinoma in rabbit. *Int J Nanomedicine*. 2022;17:5565–5579.
58. Sadasivan R, Patel A. Mono-copper substituted phosphotungstate supported on to neutral alumina: synthesis, characterization and detailed studies for oxidation of styrene. *Inorganica Chim Acta*. 2021;522:120357.
59. Yao FF, Fu WZ, Ge XH, Wang LS, Wang JH, Zhong WZ. Preparation and characterization of a copper phosphotungstate/titanium dioxide (Cu-$H_3PW_{12}O_{40}/TiO_2$) composite and the photocatalytic oxidation of high-concentration ammonia nitrogen. *Sci Total Environ*. 2020;727:138425.
60. Xie F, Li X, Li YJ, Jiang XS, Rui Q, Sha JQ. Assembly of polyoxometalate-templated metal-organic framework with effective peroxidase-like catalytic activity. *J Coord Chem*. 2019;72(2):272–282.
61. Han XX, Huang J, Jing XX, et al. Oxygen-deficient black titania for synergistic/enhanced sonodynamic and photoinduced cancer therapy at near infrared-II biowindow. *ACS Nano*. 2018;12(5):4545–4555.
62. Yang C, Younis MR, Zhang J, Qu J, Lin J, Huang P. Programmable NIR-II photothermal-enhanced starvation-primed chemodynamic therapy using glucose oxidase-functionalized ancient pigment nanosheets. *Small*. 2020;16(25):2001518.
63. Wang JP, Sun JY, Wang YH, et al. Gold nanoframeworks with mesopores for raman-photoacoustic imaging and photo-chemo tumor therapy in the second near-infrared biowindow. *Adv Funct Mater*. 2020;30(9):1908825.
64. Jiang YY, Li JC, Zhen X, Xie C, Pu KY. Dual-peak absorbing semiconducting copolymer nanoparticles for first and second near-infrared window photothermal therapy: a comparative study. *Adv Mater*. 2018;30(14):1705980.